Ultrasound-induced lung hemorrhage is not caused by inertial cavitation

William D. O'Brien, Jr.[a] and Leon A. Frizzell
Bioacoustics Research Laboratory, Department of Electrical and Computer Engineering, University of Illinois, 405 North Mathews, Urbana, Illinois 61801

Ronald M. Weigel and James F. Zachary
Department of Veterinary Pathobiology, University of Illinois, 2001 South Lincoln Avenue, Urbana, Illinois 61802

(Received 15 February 2000; accepted for publication 21 May 2000)

In animal experiments, the pathogenesis of lung hemorrhage due to exposure to clinical diagnostic levels of ultrasound has been attributed to an inertial cavitation mechanism. The purpose of this article is to report the results of two experiments that directly contradict the hypothesis that ultrasound-induced lung hemorrhage is caused by inertial cavitation. Elevated hydrostatic pressure was used to suppress the involvement of inertial cavitation. In experiment one, 160 adult mice were equally divided into two hydrostatic pressure groups (0.1 or 1.1 MPa), and were randomly exposed to pulsed ultrasound (2.8-MHz center frequency, 1-kHz PRF, 1.42-μs pulse duration, 10-s exposure duration). For the two hydrostatic pressure groups (80 mice each), 8 *in situ* peak rarefactional pressure levels were used that ranged between 2.82 and 11.8 MPa (10 mice/group). No effect of hydrostatic pressure on the probability of hemorrhage was observed. These data lead to the conclusion that lung hemorrhage is not caused by inertial cavitation. Also, the higher hydrostatic pressure enhanced rather than inhibited the impact of ultrasonic pressure on the severity (hemorrhage area, depth, and volume) of lesions. These counterintuitive findings were confirmed in a second experiment using a 2×5 factorial design that consisted of two ultrasonic pressure levels and five hydrostatic pressure levels (100 mice, 10 mice/group). If inertial cavitation were the mechanism responsible for lung hemorrhage, then elevated hydrostatic pressures should have resulted in less rather than more tissue damage at each ultrasonic pressure level. This further supports the conclusion that the pathogenesis of ultrasound-induced lung hemorrhage is not caused by inertial cavitation. © *2000 Acoustical Society of America.* [S0001-4966(00)01309-6]

PACS numbers: 43.80.Gx, 43.25.Yw [FD]

INTRODUCTION

The clinical use of diagnostic ultrasound has had a remarkable safety record with no reported adverse effects in human beings. However, concerns for its safety have been raised recently following the publication of experimental findings documenting lung hemorrhage in mice,[1–5] rats,[6] rabbits,[4,5] monkeys,[7] and pigs[8–10] at levels of ultrasound exposure and pulsing conditions consistent with those used for ultrasonography in human beings. Thus there are questions of fundamental clinical significance regarding the safe use of ultrasonography. Can diagnostic ultrasound produce lung damage in human beings and, if so, under what exposure conditions does the damage affect pulmonary function? Credible answers to these questions must come from *in vivo* laboratory animal studies that are focused on the mechanical and biological mechanisms responsible for ultrasound-induced lung hemorrhage. Comparisons of *in vivo* studies on the safety of ultrasound, using animal species with lung structure and function similar and dissimilar to human beings, can provide the scientific basis for extrapolation to human beings.

Exposure to ultrasound can produce thermal and nonthermal effects that alter tissue integrity and cellular function. Heating results from absorption, the transfer of mechanical energy from the ultrasound wave to tissue, and the failure of tissue to dissipate that energy efficiently. A rise in the temperature of several degrees Celsius can result in cell injury ranging from altered function of enzyme systems to coagulation of cellular proteins and cell death. However, several studies have indicated that heating is not responsible for ultrasound-induced lung hemorrhage.[1,2]

Nonthermal effects in lung could occur through both cavitational and noncavitational mechanisms. Inertial cavitation (cavitational mechanism) involves the growth and collapse of small microbubbles (and requires the presence of cavitation nuclei-stabilized gas microbubbles) at ultrasonic pressures typical of medical ultrasound. Other mechanical effects (noncavitational mechanisms) can occur in the presence of larger gas bodies within tissues or in tissues lacking cavitation nuclei. Noncavitational mechanisms include radiation force, radiation torque, and microstreaming and can cause tissue injury due to stress and shearing.[11]

Studies on ultrasound exposure conducted over the past decade have provided indirect evidence implicating cavitation in the pathogenesis of lung hemorrhage.[1,6,7,11] Aeration of the lung is necessary to produce hemorrhage.[2] Because of air in alveoli, it has been hypothesized that small bubbles

[a]Electronic mail: wdo@uiuc.edu

TABLE I. Experiment 1 ultrasonic exposure levels for the 0.1- and 1.1-MPa hydrostatic pressure study. The means of the axial maximum water-based values of the peak rarefactional $p_{r(in\ vitro)}$ and peak compressional $p_{c(in\ vitro)}$ ultrasonic pressures are reported for a hydrostatic pressure of 0.1 MPa. The estimated *in situ* (at the pleural surface) values of the peak rarefactional $p_{r(in\ situ)}$ and peak compressional $p_{c(in\ situ)}$ ultrasonic pressures are reported for both hydrostatic pressure conditions. The Mechanical Index is determined according to the ODS procedures (Ref. 28). The pulse repetition frequency was 1 kHz for all exposure conditions except the sham-exposure conditions for which the PRF was 10 Hz.

Number of mice (0.1-MPa Hydrostatic pressure)	Number of mice (1.1-MPa Hydrostatic pressure)	$p_{r(in\ vitro)}$ (0.1-MPa Hydrostatic pressure) (MPa)	$p_{c(in\ vitro)}$ (0.1-MPa Hydrostatic pressure) (MPa)	$p_{r(in\ situ)}$ (0.1-MPa Hydrostatic pressure) (MPa)	$p_{c(in\ situ)}$ (0.1-MPa Hydrostatic pressure) (MPa)	Mechanical index (0.1-MPa hydrostatic pressure)	$p_{r(in\ situ)}$ (1.1-MPa Hydrostatic pressure) (MPa)	$p_{c(in\ situ)}$ (1.1-MPa Hydrostatic pressure) (MPa)
15 (sham)	15 (sham)	0.28	0.28	0.25	0.26	0.14	[a]	[a]
10	-	3.13	3.46	2.82	3.12	1.54	-	-
10	10	4.19	4.46	3.78	4.02	2.06	3.42	3.64
10	-	5.33	6.24	4.99	5.63	2.72	-	-
10	10	6.42	7.20	5.79	6.50	3.15	5.24	5.88
10	10	7.49	8.35	6.76	7.53	3.67	6.11	6.81
10	10	9.02	10.8	8.14	9.77	4.40	7.37	8.84
10	10	10.2	13.0	9.21	11.8	4.97	8.33	10.6
10	10	11.4	15.1	10.2	13.6	5.51	9.26	12.3
-	10	12.8	19.9	-	-	6.16	10.5	16.3
-	10	14.5	22.9	-	-	6.96	11.8	18.7

[a]Positioning of the ultrasound focal region on the lung surface was done at a hydrostatic pressure of 0.1 MPa prior to the mouse being placed in the hyperbaric chamber. This procedure was required to maintain blinded exposures so that the mouse handler did not know the hydrostatic pressure condition.

(1–5 μm in diameter) may exist in the surfactant layer and serve as cavitation nuclei.[7] If cavitation nuclei are present, then exposure of these gas bubbles to high ultrasonic stresses may result in their violent oscillation and rapid collapse, a process known as inertial cavitation. Under these conditions, the motion of the gas–liquid interface may reach supersonic speeds (producing shock waves) and bubble collapse may generate chemically reactive free radicals, extremely high temperatures, and microjets, which could easily damage the air–blood barrier resulting in lung hemorrhage.[11] As a result, investigators have suggested that inertial cavitation is the mechanism responsible for lung hemorrhage in at least mice,[1] rats,[6] and monkeys,[7] and it is thus important to determine conclusively if inertial cavitation is the mechanism responsible for lung hemorrhage.

The purpose of this article is to report the results of a series of experiments that directly contradict the view that ultrasound-induced lung hemorrhage is caused by inertial cavitation. To test whether inertial cavitation was responsible for lung damage, this study was designed to determine if overpressure (i.e., increased hydrostatic pressure) could suppress lung damage. Increased hydrostatic pressure has been used to suppress cavitation in studies of the biological effects of ultrasound,[3,12–18] as well as to suppress cavitation associated with extracorporeal shock waves.[19–21] The effect of the overpressure may be to reduce or eliminate the negative total pressure during the pulse, which will increase the threshold for inertial cavitation.[22,23] However, overpressures that were small compared to the peak negative pressure associated with lithotripsy pulses have been shown to reduce or eliminate inertial cavitation *in vitro*,[19–21] and it has been suggested that this may be associated with the elimination of cavitation nuclei.[20,21] Regardless of the mechanism, these studies utilized the fact that elevated hydrostatic pressure increases the cavitation threshold, or suppresses cavitation.[24–27]

I. MATERIALS AND METHODS

A. Animal handling and experimental design

Two experiments were conducted. The second experiment was designed to test counterintuitive findings from the first experiment. The experimental protocols were approved by the campus' Laboratory Animal Care Advisory Committee and satisfied all campus and NIH rules for the humane use of laboratory animals. Animals were housed in an AAALAC approved animal facility, placed in groups of four in polycarbonate cages, and provided food and water *ad libitum*.

For experiment 1 (Table I[28]) there were a total of 190 six-to-seven-week-old 27.8 ± 2.1-g female ICR mice (Harlen Sprague Dawley Laboratories, Indianapolis, IN). One hundred and sixty mice were divided ($n = 80$/group) into two hydrostatic pressure groups [0.1 MPa (1 atm) and 1.1 MPa (11 atm)]. Each hydrostatic pressure group was subdivided into eight-ultrasonic pressure groups consisting of ten mice per group. The other 30 mice were divided ($n = 15$/group) into the 2 hydrostatic pressure groups and were the sham-exposed animals.

For experiment 2 (Table II) there were a total of 115 six-to-seven-week-old 26.8 ± 3.1-g female ICR mice (Harlen Sprague Dawley Laboratories, Indianapolis, IN). One hundred mice were divided ($n = 10$/group) into ten groups based on a 2×5 factorial design. There were two *in situ* peak rarefactional pressure groups (6.0 and 10.9 MPa) and five hydrostatic pressure groups (0.1, 0.4, 0.7, 1.0, and 1.3 MPa). The other 15 mice were divided ($n = 3$/group) into the 5 hydrostatic pressure groups and were the sham-exposed animals.

For both experiments, animals were assigned to each hydrostatic pressure group and ultrasonic pressure group at random. The sham-exposed animals were incorporated into the randomization. The individuals involved in animal han-

TABLE II. Experiment 2 ultrasonic exposure levels at the five hydrostatic pressure levels. The means of the axial maximum water-based values of the peak rarefactional $p_{r(in\ vitro)}$ and peak compressional $p_{c(in\ vitro)}$ ultrasonic pressures are reported for a hydrostatic pressure of 0.1 MPa. The estimated *in situ* (at the pleural surface) values of the peak rarefactional $p_{r(in\ situ)}$ and peak compressional $p_{c(in\ situ)}$ ultrasonic pressures are reported at the indicated hydrostatic pressure levels. The Mechanical Index is determined according to the ODS procedures (Ref. 28). The pulse repetition frequency was 1 kHz for all exposure conditions except the sham exposure conditions for which the PRF was 10 Hz.

Number of mice	Hydrostatic pressure (MPa)	$p_{r(in\ vitro)}$[a] (MPa)	$p_{c(in\ vitro)}$[a] (MPa)	$p_{r(in\ situ)}$ (MPa)	$p_{c(in\ situ)}$ (MPa)	Mechanical index[a]
15 (sham)	0.1	0.28	0.28	0.25[b]	0.25[b]	0.14
10	0.1	6.45	7.26	5.95	6.69	3.09
10	0.4	6.70	7.79	5.99	6.96	3.21
10	0.7	7.09	8.60	6.05	7.34	3.39
10	1.0	7.22	8.87	6.07	7.48	3.45
10	1.3	7.22	8.87	6.07	7.48	3.45
10	0.1	11.7	18.3	10.8	16.8	5.52
10	0.4	12.2	19.2	10.9	17.1	5.72
10	0.7	12.8	20.5	10.9	17.5	6.02
10	1.0	13.0	20.9	11.0	17.7	6.11
10	1.3	13.0	20.9	11.0	17.7	6.11

[a]$p_{r(in\ vitro)}$, $p_{c(in\ vitro)}$, and Mechanical Index are reported at 0.1-MPa hydrostatic pressure.
[b]Positioning of the ultrasound focal region on the lung surface was done at a hydrostatic pressure of 0.1 MPa prior to the mouse being placed in the hyperbaric chamber. This procedure was required to maintain blinded exposures so that the mouse handler did not know the hydrostatic pressure condition.

dling, exposure, and lesion scoring were blinded to the exposure conditions. The exposure conditions were revealed only after the final results were tabulated.

Mice were weighed and then anesthetized with ketamine hydrochloride (125.0 mg/kg) and xylazine (25.0 mg/kg) administered intraperitoneally. For each animal, the skin of the left thorax was exposed by removing the hair with an electric clipper, followed by a depilatory agent (Nair®, Carter-Wallace, Inc., New York, NY) to maximize sound transmission. A black dot was placed on the skin at approximately the sixth to ninth rib. The anesthetized animal was placed in a specially designed holder, to which the ultrasonic transducer was attached. A removable pointer, attached to the transducer, was used to position the ultrasonic beam perpendicular to the skin at the position of the black dot and in the beam's focal region.

The holder was placed in a separate degassed, temperature-controlled (30 °C) water tank for transducer positioning. The transducer was not in direct contact with the mouse. Water served as the coupling medium between the ultrasound transducer and the mouse in order to align the transducer's focal region on the pleural surface. The low-power pulse-echo signal of the exposure system (RAM 5000, Ritec, Inc., Warwick, RI) displayed on an oscilloscope was used to adjust the transducer's axial position so that the focal region was within 1 mm of the lung surface. The low-power exposure conditions were as follows: 2.8-MHz center frequency, 10-Hz pulse repetition frequency, 1.42-μs pulse duration, 5–20-s exposure duration (see sham in Tables I and II for these low-level ultrasonic pressure levels). The lung surface provided distinctive echo characteristics that allowed for the precise positioning of the focal region of the ultrasound beam on the pleural surface. The holder was then removed from this separate water tank and placed in a specially fabricated hyperbaric chamber,[12,16,17] and the animal was exposed to pulsed ultrasound (2.8-MHz center frequency, 1-kHz pulse repetition frequency, 1.42-μs pulse duration, 10-s exposure duration). For animals exposed at the elevated hydrostatic pressure, the hydrostatic pressure was increased to its maximum level in about 6 min and then decreased back to 0.1 MPa in about 4 min, a procedure that was adhered to for all animals. Following the ultrasound exposure procedure, the animal was removed from the chamber and holder, and euthanized under anesthesia by cervical dislocation.

The 2.8-MHz center frequency was used since it was within the lower end of the diagnostic ultrasound frequency range. The 10-s exposure duration was used to simulate incidental exposure to lung tissue since, in clinical practice, the lung is generally not intentionally exposed to diagnostic ultrasound.

The thorax was opened, and the thickness of each left thoracic wall (skin, rib cage, and parietal pleura) at the point of exposure was measured (experiment 1: 2.89 ± 0.90 mm for all 190 mice; experiment 2: 2.32 ± 0.36 mm for all 115 mice) using a digital micrometer (accuracy: 10 μm). These chest wall measurements were used for later calculation of the *in situ* ultrasonic pressures at the visceral pleural surface (Tables I and II). The lungs were removed from each animal, and the left lung lobe was scored for the presence or absence of hemorrhage. Lung hemorrhage formed along the pathway of the ultrasound beam, and the lesion assumed a conical shape. The base of the lesion originated at the visceral pleural surface and was elliptical in shape. The lesion extended into lung parenchyma to form its apex at varied depths within the lung. The left lung was fixed by immersion in 10% neutral-buffered formalin for a minimum of 24 h. After fixation, the elliptical dimensions of each lung lesion at the visceral pleural surface were measured using a digital micrometer where ''*a*'' is the semi-major axis and ''*b*'' is the semi-minor axis. The lesion was then bisected and the depth

''*d*'' of the lesion within the pulmonary parenchyma was also measured. The surface area (πab) and volume ($\pi abd/3$) of the lesion were calculated for each animal. Each half of the bisected lesion was embedded in paraffin, sectioned at 5 μm, stained with hematoxylin and eosin, and evaluated microscopically.

B. Transducer characteristics and ultrasound field calibrations

Ultrasonic exposures were conducted for both experiments using a focused, 19-mm-diameter, $f/1$, lithium niobate ultrasonic transducer (Valpey Fisher, Hopkinton, MA). Pulse-echo field distribution measurements[29] in degassed water yielded the following transducer characteristics: 2.8-MHz center frequency, 11.6% fractional bandwidth, 18.9-mm focal length, 466-μm, 6-dB beamwidth at the focus, 2.73-mm, 6-dB depth of focus.

A special procedure was developed to routinely calibrate the ultrasound fields in degassed water. This procedure was based on accepted national standards.[28,30] The source transducer's drive voltage was supplied by Ritec's RAM5000 that has the capability to deliver up to a 5-kW single-cycle pulse into a 50-ohm load. An automated search procedure was developed to determine the beam axis at each drive voltage.[31] This search procedure was based on the maximum value of the pulse intensity integral (PII). The maximum PII value was determined at various axial positions using a computer-controlled micropositioning system (three orthogonal axes, each with a linear accuracy of 2 μm). The coordinates of these maximum PII values were used to determine the beam axis using a linear regression procedure. The same calibrated hydrophone used to determine the beam axis was scanned along the beam axis and through the focal region at 50-μm intervals. At each interval, the rf hydrophone waveform was digitized (500 Ms/s, LeCroy Model 9354TM, Chestnut Ridge, NY). These digitized hydrophone waveforms were processed off-line (Matlab®, Natick, MA) on a Sun UltraSparc workstation to yield the following axial profiles: rarefactional pressure, compressional pressure, pulse intensity integral, and their respective derated (0.3-dB/cm MHz) profiles. Twelve independent axial calibrations were conducted over the two-month period of the experiments using two calibrated PVDF membrane hydrophones (Sonic Technologies Model 804-010, Hatboro, PA and Marconi Model Y-34-6543, Chelmsford, U.K.); standard deviations were less than 15% of their respective mean values. The water-based exposure quantities determined from the calibrated axial profiles were the maximum values of the peak rarefactional $p_{r(in\ vitro)}$ and peak compressional $p_{c(in\ vitro)}$ ultrasonic pressures (Tables I and II). The axial locations of $p_{c(in\ vitro)}$ and $p_{r(in\ vitro)}$ were determined, and their axial differences ranged from about 10 μm for the sham-exposure level to about 800 μm for the highest exposure level. The Mechanical Index was calculated using the ODS procedure[28] from $p_{r.3}/\sqrt{f_c}$, where $p_{r.3}$ is the peak rarefactional pressure derated by 0.3 dB/cm MHz at the location where the derated pulse intensity integral $PII_{0.3}$ is a maximum and f_c is the center frequency of 2.8 MHz.

The *in situ* (at the pleural surface) peak rarefactional pressure levels were estimated from

$$p_{r(in\ situ)} = T \cdot p_{r(in\ vitro)} e^{-(A \cdot x)}, \tag{1}$$

where $p_{r(in\ vitro)}$ is the maximum peak rarefactional pressure at 0.1-MPa hydrostatic pressure, ''*A*'' is the mean attenuation coefficient of the chest wall (3.10 ± 0.86 dB/cm at 2.8 MHz; Ref. 32) measured from 35 separate chest walls using a broadband through-transmission insertion loss technique,[33] and ''*x*'' is the mean chest wall thickness (2.89 ± 0.90 mm). The transducer's relative pressure efficiency ''*T*'' was determined by operating the Ritec's RAM5000 in its pulse-echo mode. The 2.8-MHz transducer was placed in the hyperbaric chamber, and the echo amplitude reflected from a stainless steel reflector (oriented normal to the beam axis with the focus at the reflector surface) was measured as a function of hydrostatic pressure (from 0.1 to 1.45 MPa in 0.15-MPa increments). Five Ritec drive voltage levels were used that bracketed the ultrasonic pressure levels of both animal experiments. The pressure efficiency experiment was conducted on two different days, and there was no apparent difference between the two data sets. Therefore, the pulse-echo amplitude results at each drive voltage were averaged for each hydrostatic pressure level. The pulse-echo amplitude results as a function of hydrostatic pressure were normalized to that at a hydrostatic pressure of 0.1 MPa to yield the squared relative pressure efficiency T^2. For experiment 1, two hydrostatic pressures were used for which $T = 1.00$ (0.1 MPa) and 0.91 (1.1 MPa). For experiment 2, five hydrostatic pressures were used for which $T = 1.00$ (0.1 MPa), 0.97 (0.4 MPa), 0.93 (0.7 MPa), 0.91 (1.0 MPa), and 0.91 (1.3 MPa). The results reported herein are in terms of $p_{r(in\ situ)}$ (Tables I and II).

II. RESULTS

Sham-exposed mice were included in the randomized designs of both experiments. These mice received low-level ultrasonic exposure (see Tables I and II) during the beam alignment procedure. Thirty sham-exposed mice were included in the first experiment, fifteen for each hydrostatic pressure condition. Fifteen sham-exposed mice were included in the second experiment, three for each hydrostatic pressure condition. In all cases, none of the sham-exposed mice demonstrated lung hemorrhages.

Data analyzed for each animal included the presence or absence of a lesion, the lesion surface area, and the lesion depth. Lesion volume was not statistically analyzed as an outcome because it did not provide information independent of lesion area and depth. The effects of $p_{r(in\ situ)}$ and hydrostatic pressure, and the interaction of these factors, upon the presence or absence of a lesion (percentage of animals with lung lesions) were analyzed using multiple logistic regression analysis[34] (Fig. 1). There was no significant difference in percentage of lesions between the two hydrostatic pressure groups.

The effects of $p_{r(in\ situ)}$ and hydrostatic pressure, and the interaction of these factors, upon lesion surface area and depth were analyzed using multiple linear regression analysis[35] (Fig. 2). At low ultrasonic pressures, lesions were

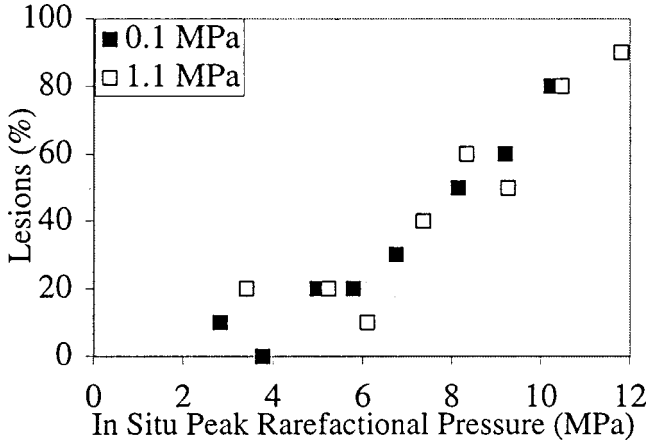

FIG. 1. Percentage of lesions ($n=10$/group) as a function of $p_{r(in\ situ)}$ at hydrostatic pressures of 0.1 and 1.1 MPa for experiment 1. The multiple logistic regression analysis (model $\chi^2=101.4$; $p<0.0001$) indicates there was no apparent effect of hydrostatic pressure on whether or not a lesion occurred. However, increased $p_{r(in\ situ)}$ was associated with an increased probability of a lesion occurring ($p<0.0001$). There was no apparent interaction between the experimental factors.

nonexistent or small, and there were no significant effects due to hydrostatic pressure. As $p_{r(in\ situ)}$ increased, lesion area and depth increased. Increase in lesion area with increased $p_{r(in\ situ)}$ occurred at a greater rate at 1.1-MPa hydrostatic pressure than at 0.1-MPa hydrostatic pressure. With respect to lesion depth, there was no significant effect of hydrostatic pressure or an interaction of $p_{r(in\ situ)}$ with hydrostatic pressure. These data indicate that increases in hydrostatic pressure enhance (rather than inhibit) lesion surface area; however, hydrostatic pressure did not appear to modify the effect of $p_{r(in\ situ)}$ in penetrating lung tissue.

Based on the results of experiment 1, a second experiment was conducted to confirm the counterintuitive findings. The second experiment had a 2×5 factorial design (two $p_{r(in\ situ)}$ levels and five hydrostatic pressure levels). One of the $p_{r(in\ situ)}$ levels (6.0 MPa) was selected to be near but slightly greater than the 5.5-MPa $p_{r(in\ situ)}$ crossover point of the two regression lines from the first study [Figs. 2(A) and 2(B)], where no substantial hydrostatic pressure effect was noted. The other $p_{r(in\ situ)}$ level (10.9 MPa) was selected to be much higher, where the hydrostatic pressure level was observed to affect lesion size. The water-based calibrated value of $p_{r(in\ vitro)}$ was varied in order to keep $p_{r(in\ situ)}$ constant at either 6.0 MPa or 10.9 MPa for each of the hydrostatic pressure levels.

If the relationships identified in experiment 1 were replicated, then lesion depth and surface area would increase with higher $p_{r(in\ situ)}$, and for lesion area these differences would be predicted to be greater as hydrostatic pressures increased. This prediction was supported in part. The results of experiment 2 confirmed an increase in the probability of a lesion, lesion area, and lesion depth with increasing ultrasonic pressure. There were new findings in the second experiment. Increased hydrostatic pressure was associated with increased probability of a lesion (Fig. 3) and increased lesion depth (Fig. 4). However, in contrast to the first experiment, there was no interaction between $p_{r(in\ situ)}$ and hydrostatic

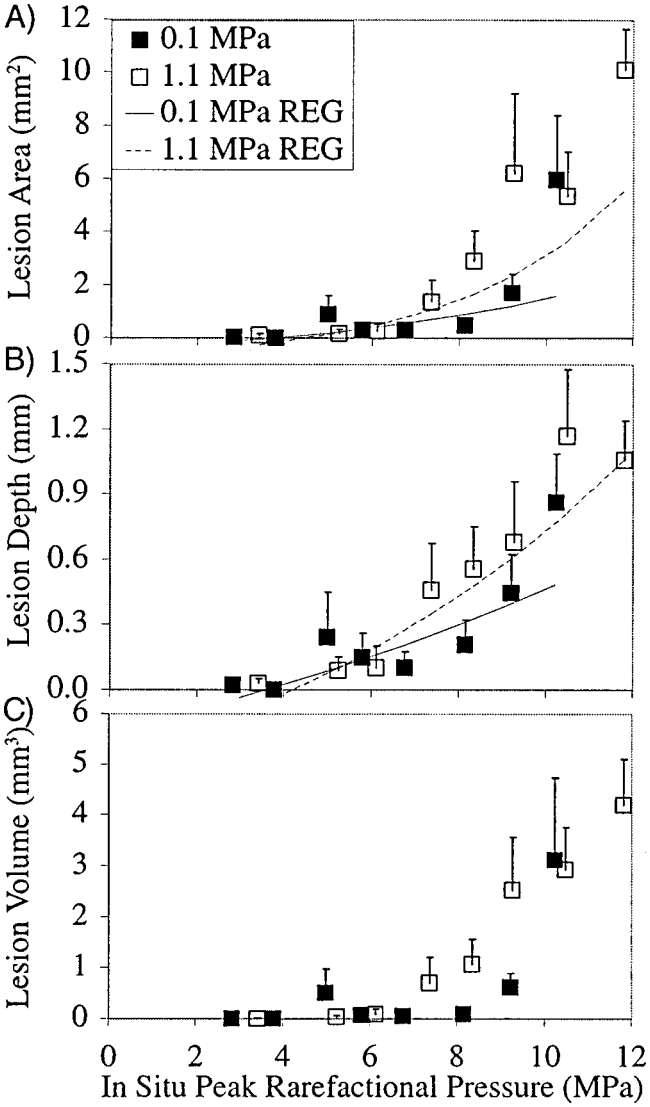

FIG. 2. Mean lesion area (A), depth (B), and volume (C) as a function of $p_{r(in\ situ)}$ at hydrostatic pressures of 0.1 and 1.1 MPa for experiment 1. Error bars (shown in only one direction) represent standard error. The fitted lines are regression functions determined from natural log transformation [ln(measure+1)] of lesion area and depth as a function of $p_{r(in\ situ)}$ at hydrostatic pressures of 0.1 (solid line) and 1.1 (dashed line) MPa for all 160 mouse lungs (16 groups with 10 mice/group). The logarithmic transformation of lesion area and depth was conducted to correct for nonnormality and heterogeneity of residual variance. The linear regression analysis indicated there was an interaction between $p_{r(in\ situ)}$ and hydrostatic pressure in affecting lesion surface area ($p=0.017$). There was no significant interaction between $p_{r(in\ situ)}$ and hydrostatic pressure in affecting lesion depth ($p=0.12$). Lesion depth increased with increasing ultrasonic pressure ($p<0.0001$). [Model $R^2=0.39$ for surface area; $=0.31$ for depth.]

pressure, although the main effect of $p_{r(in\ situ)}$ in increasing lesion area was still apparent (Fig. 4). This lack of interaction between $p_{r(in\ situ)}$ and hydrostatic pressure suggests that the effects are additive from the individual observations ($p_{r(in\ situ)}$ and/or hydrostatic pressure).

III. DISCUSSION

A considerable amount of work has been published regarding lung hemorrhage caused by ultrasound.[11] There is agreement that gas in the lung plays a role in the ultrasound-induced damage mechanism, and that the mechanism is non-

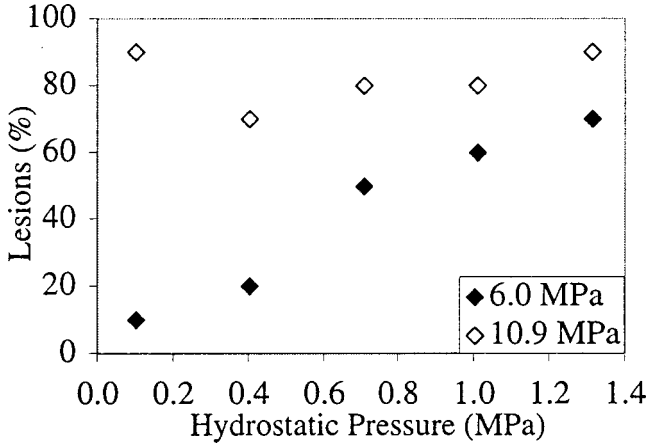

FIG. 3. Percentage of lesions ($n=10$/group) as a function of hydrostatic pressure at $p_{r(in\ situ)}$ values of 6.0 and 10.9 MPa for experiment 2. The multiple logistic regression analysis (model $\chi^2=35.7$; $p<0.0001$) indicates that the probability of a lesion increased with increasing $p_{r(in\ situ)}$ ($p<0.0001$) and with increasing hydrostatic pressure ($p=0.004$), but there was no significant interaction effect for these experimental factors ($p=0.066$).

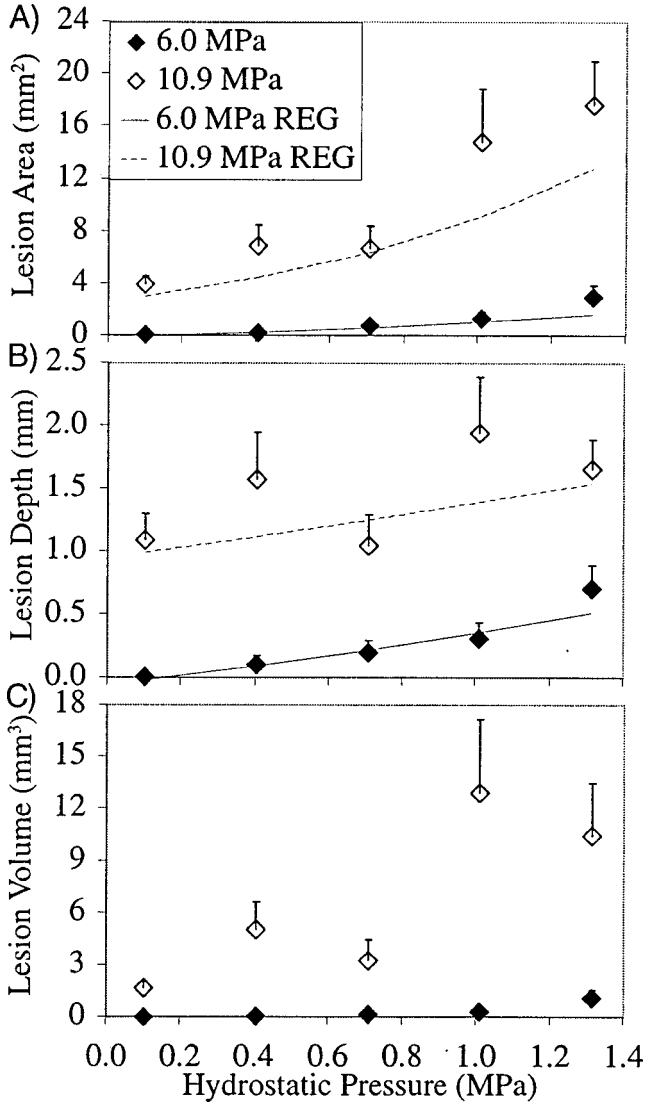

FIG. 4. Mean lesion area (A), depth (B), and volume (C) as a function of hydrostatic pressure at $p_{r(in\ situ)}$ values of 6.0 and 10.9 MPa for experiment 2. Error bars (shown in only one direction) represent standard error. The fitted lines are regression functions determined from natural log transformation [ln(measure+1)] of lesion area and depth as a function of hydrostatic pressures at $p_{r(in\ situ)}$ values of 6.0 (solid line) and 10.9 (dashed line) MPa for all 100 mouse lungs (10 groups with 10 mice/group). The logarithmic transformation of lesion area and depth was conducted to correct for non-normality and heterogeneity of residual variance. The linear regression analysis indicated that both increasing $p_{r(in\ situ)}$ and hydrostatic pressure increased the lesion area [$R^2=0.57$], and lesion depth [$R^2=0.47$] [both p values <0.0001]. However, the interaction effect between $p_{r(in\ situ)}$ and hydrostatic pressure in affecting lesion surface area was not apparent. Ultrasound exposure contributed most to the lesion surface area (accounting for 45% of the variance in surface area and 41% of the variance in lesion depth).

thermal. However, a distinction must be made between mechanisms involving large gas bodies, such as gas in the alveoli of the lung (38–49 μm; Refs. 36–38), and classical inertial cavitation that involves small microbubbles as nuclei (radii on the order of 1 μm or less; Ref. 39). Evidence has been slowly accumulating that suggests that the mechanism of damage in the lung is not inertial cavitation. There seems to be no dependence on whether the negative or positive pressure components of the ultrasonic pulse cause lithotripter-induced lung damage whereas inertial cavitation is associated with the negative pressure.[40] The frequency dependence may not be the same as that associated with effects due to the presence of contrast agents that quite clearly nucleate inertial cavitation.[41]

These two experiments using overpressure to suppress inertial cavitation indicate quite conclusively that inertial cavitation is not responsible for the lung damage. If inertial cavitation were the responsible mechanism, then the higher hydrostatic pressure results would have resulted in lower rather than higher tissue damage at each $p_{r(in\ situ)}$ level. The interaction identified in this study indicates that the mechanism is more complex. At low $p_{r(in\ situ)}$ (around 5.5 MPa), there was no apparent effect of hydrostatic pressure on lung hemorrhage. As $p_{r(in\ situ)}$ increased, lesions became more common and larger in area and depth, and hence volume. At these higher ultrasonic pressures, a modifying effect of hydrostatic pressure became apparent. However, instead of inhibiting lung hemorrhage, higher hydrostatic pressure enhanced damage (as indicated by higher lesion areas, depths, and volumes) (Figs. 2 and 4), with this enhancement of hemorrhage increasing with increasing $p_{r(in\ situ)}$.

The absence of lung damage at low $p_{r(in\ situ)}$ levels for both hydrostatic pressures from experiment 1 (Figs. 1 and 2) suggests there is a threshold for ultrasound-induced lung hemorrhage that is independent of hydrostatic pressure. The imperceptible differences in the level of damage at the lowest $p_{r(in\ situ)}$ levels, however, makes the determination of a threshold (ultrasonic pressure level at which there is no effect) difficult. In any case, an approximate range of thresholds can be estimated from the results reported herein. It must be emphasized, however, that the basic experimental design was not intended to identify definitive thresholds. Best-fit straight lines for the two hydrostatic pressure data sets (using eight values each of Fig. 1) yielded $p_{r(in\ situ)}$ intercepts of 3.1 and 3.0 MPa for 0.1- and 1.1-MPa hydrostatic pressures, respectively. It is clear from Fig. 1 that the $p_{r(in\ situ)}$ threshold is less than 3 MPa and therefore an esti-

mated threshold range around 2.0 MPa seems more reasonable. This value is slightly greater than the values reported by others[1,42] with adult mice near this ultrasonic frequency using longer exposure durations.

The results shown in Fig. 1 indicate that the $p_{r(in\ situ)}$ threshold for hemorrhage occurrence was approximately the same at hydrostatic pressures of 0.1 and 1.1 MPa. This finding leads to the conclusion that the initiation of lung hemorrhage is not caused by inertial cavitation. Even though the hydrostatic pressures used were not large enough to completely eliminate a negative total pressure, based on previous work *in vitro*[19] and *in vivo*,[3] these levels were sufficient to significantly change the threshold for effects of inertial cavitation, should it occur.

It is interesting that the hemorrhage areas, depths, and volumes were greater under increased hydrostatic pressure, which initially seems counterintuitive. Recent studies[20,21] have shown that increased hydrostatic pressure can increase the damage caused by cavitation on metal foils where cavitation nuclei are trapped in crevices. However, these same studies showed that inertial cavitation effects on cells were eliminated by overpressure in the absence of the metal foils. These data lead us to suggest that some other phenomenon must be responsible for the enhanced effects on hemorrhage at the higher hydrostatic pressure.

The change in acoustic impedance difference between intercostal tissue and lung was evaluated as a possible explanation for the enhanced lung damage with increased hydrostatic pressure. A planar boundary was assumed between intercostal tissue and lung with the incident ultrasonic field in the intercostal tissue and the ultrasonic beam axis normal to the boundary. Lung was modeled as two components consisting of air and parenchyma where density

$$\rho_{\text{lung}} = x_{\text{air}}\rho_{\text{air}} + x_{\text{parenchyma}}\rho_{\text{parenchyama}} \tag{2}$$

and adiabatic bulk modulus

$$B_{\text{lung}} = x_{\text{air}}B_{\text{air}} + x^{3.5}_{\text{parenchyama}}B_{\text{parenchyama}}, \tag{3}$$

and where the volume fractions are $x_{\text{air}} + x_{\text{parenchyma}} = 1$. This model was selected because it fit the experimental measurements of reflection coefficient versus lung inflation in the fixed lungs of dogs at 2.4 MHz[43] and the experimental measurements of propagation speed at one lung inflation in fresh lungs of dogs at 2.25 MHz.[44] These published measurements, of course, were all conducted at atmospheric pressure (0.1 MPa). The fit to these published measurements yielded $\rho_{\text{air}} = 1.21\ \text{kg/m}^3$, $\rho_{\text{parenchyma}} = 600\ \text{kg/m}^3$, $B_{\text{air}} = 142\ \text{kPa}$, and $B_{\text{parenchyma}} = 1\ \text{GPa}$ for $x_{\text{air}} = 0.31$, and, in turn, yielded $\rho_{\text{lung}} = 414\ \text{kg/m}^3$ and $B_{\text{lung}} = 273\ \text{MPa}$. Propagation speed is determined from $c_{\text{lung}} = \sqrt{B_{\text{lung}}/\rho_{\text{lung}}}$, and impedance from $z_{\text{lung}} = \sqrt{\rho_{\text{lung}}B_{\text{lung}}}$. These fit values agreed well with published results. The fit reflection coefficient value relative to 1.5 Mrayl was -7.7 dB; the published values were between -2 and -4 dB.[43] The fit and published[44] lung propagation speed values were 812 m/s. As hydrostatic pressure increased from 0.1 to 1.3 MPa, ρ_{air} increased from 1.21 to 15.7 kg/m^3 and B_{air} from 0.142 to 1.85 MPa (ideal gas law), but ρ_{lung} increased slightly from 414 to 419 kg/m^3 and c_{lung} decreased slightly from 812 to 808 m/s which resulted in only a slight increase in z_{lung} from 336 to 338 krayl. Since the intercostal tissue is reasonably modeled as incompressible, it is shown that there is essentially no change in the reflection and transmission coefficients as a function of hydrostatic pressure at a constant lung inflation (constant $x_{\text{air}} = 0.31$). It is interesting to note that under these conditions, the sound power transmission coefficient is 41%, indicating that 41% of the incident power at the intercostal tissue-lung boundary is transmitted into lung. Thus as a function of hydrostatic pressure, this impedance difference alone cannot explain the enhanced effects on hemorrhage at the higher hydrostatic pressure.

If the mouse's breathing pattern was somehow altered as a function of hydrostatic pressure, and this alteration affected the volume of air inspired and expired, a supposition, then an increase in the power transmitted into lung might occur. From the above two-component lung model at 0.1-MPa hydrostatic pressure, if the volume fraction of air x_{air} varied between 0.25 and 0.40, then the respective sound power transmission coefficient would vary between 66% and 48%. If the increased hydrostatic pressure caused the mouse to expire more air, and hence result in $x_{\text{air}} < 0.25$, then the sound power transmission coefficient would be greater than 66% at maximum expiration, i.e., at $x_{\text{air}} = 0.20$, 72% of the incident power at the intercostal tissue-lung boundary would be transmitted into lung. For this supposition to account for the enhanced lung damage at increased hydrostatic pressure, the argument would also have to include a causal relationship between the sound power transmission coefficient and lung damage, one that is not yet available.

In summary, the results of these two experiments indicate that the pathogenesis of ultrasound-induced lung hemorrhage is not caused by inertial cavitation, because lung damage is not inversely correlated with hydrostatic pressure. Also, there is no significant change of the acoustic properties of lung tissue as a function of hydrostatic pressure to account for the enhanced effects of hemorrhage at elevated hydrostatic pressure.

ACKNOWLEDGMENTS

We thank G. Altmeyer, J. Blue, K. Clemens, B. McNeill, R. McQuinn, R. Miller, B. Qiao, J. Sempsrott, K. Norrell, G. Teotico, and A. Wunderlich for technical contributions. This work was supported by NIH Grant No. HL58218 awarded to WDO and JFZ.

[1] S. Z. Child, C. L. Hartman, L. A. Schery, and E. L. Carstensen, ''Lung damage from exposure to pulsed ultrasound,'' Ultrasound Med. Biol. **16**, 817–825 (1990).

[2] C. L. Hartman, S. Z. Child, R. Mayer, E. Schenk, and E. L. Carstensen, ''Lung damage from exposure to the fields of an electrohydraulic lithotripter,'' Ultrasound Med. Biol. **16**, 675–683 (1990).

[3] L. A. Frizzell, E. Chen, and C. Lee, ''Effects of pulsed ultrasound on the mouse neonate: Hind limb paralysis and lung hemorrhage,'' Ultrasound Med. Biol. **20**, 53–63 (1994).

[4] J. F. Zachary and W. D. O'Brien, Jr., ''Lung hemorrhage induced by continuous and pulse wave ultrasound in mice, rabbits, and pigs,'' Vet. Pathol. **32**, 43–54 (1995).

[5] W. D. O'Brien, Jr. and J. F. Zachary, ''Lung damage assessment from exposure to pulsed-wave ultrasound in rabbit, mouse, and pig,'' IEEE Trans. Ultrason. Ferroelectr. Freq. Control **44**, 473–485 (1997).

[6] C. K. Holland, C. X. Deng, R. E. Apfel, J. L. Alderman, L. A. Fernandez, and K. J. Taylor, ''Direct evidence of cavitation in vivo from diagnostic ultrasound'' Ultrasound Med. Biol. **22**, 917–925 (1996).
[7] A. F. Tarantal and D. R. Canfield, ''Ultrasound-Induced lung hemorrhage in the monkey,'' Ultrasound Med. Biol. **20**, 65–72 (1994).
[8] G. H. Harrison, H. A. Eddy, J.-P. Wang, and F. Z. Liberman, ''Microscopic lung alterations and reduction of respiration rate in insonated anesthetized swing,'' Ultrasound Med. Biol. **21**, 981–983 (1995).
[9] R. Baggs, D. P. Penney, C. Cox, S. Z. Child, C. H. Raeman, D. Dalecki, and E. L. Carstensen, ''Thresholds for ultrasonically induced lung hemorrhage in neonatal swine,'' Ultrasound Med. Biol. **22**, 119–128 (1996).
[10] D. Dalecki, S. Z. Child, C. H. Raeman, C. Cox, and E. L. Carstensen ''Ultrasonically induced lung hemorrhage in young swine,'' Ultrasound Med. Biol. **23**, 777–781 (1997).
[11] *Mechanical Bioeffects from Diagnostic Ultrasound: AIUM Consensus Statements* (American Institute of Ultrasound in Medicine, Laurel, MD, 2000). Also, J. Ultrasound Med. **19**, 67–168 (2000).
[12] W. J. Fry, D. Tucker, F. J. Fry, and V. J. Wulff, ''Physical factors involved in ultrasonically induced change in living systems: II. Amplitude duration relations and the effect of hydrostatic pressure for nerve tissue,'' J. Acoust. Soc. Am. **23**, 364–368 (1951).
[13] C. R. Hill, ''Ultrasonic exposure thresholds for changes in cells and tissues,'' J. Acoust. Soc. Am. **52**, 667–672 (1972).
[14] V. Ciaravino, M. W. Miller, and E. L. Carstensen, ''Pressure-mediated reduction of ultrasonically induced cell lysis,'' Radiat. Res. **88**, 209–213 (1981).
[15] K. I. Morton, G. R. terHaar, I. J. Statford, and C. R. Hill, ''Subharmonic emission as an indicator of ultrasonically-induced biological damage,'' Ultrasound Med. Biol. **9**, 629–633 (1983).
[16] C. S. Lee and L. A. Frizzell, ''Exposure levels for ultrasonic cavitation in the mouse neonate,'' Ultrasound Med. Biol. **14**, 735–742 (1988).
[17] L. A. Frizzell, C. S. Lee, P. D. Aschenbach, M. J. Borrelli, R. S. Morimoto, and F. Dunn, ''Involvement of ultrasonically induced cavitation in the production of hind limb paralysis of the mouse neonate,'' J. Acoust. Soc. Am. **74**, 1062–1065 (1983).
[18] E. C. Everbach, I. R. Makin, M. Azadniv, and R. S. Meltzer, ''Correlation of ultrasound-induced hemolysis with cavitation detector output in vitro,'' Ultrasound Med. Biol. **23**, 619–624 (1997).
[19] M. Delius, ''Minimal static excess pressure minimizes the effect of extracorporeal shock waves on cells and reduces it on gallstones,'' Ultrasound Med. Biol. **23**, 611–617 (1997).
[20] J. A. McAteer, M. A. Stonehill, K. Colmenares, J. C. Williams, A. P. Evan, R. O. Cleveland, M. R. Bailey, and L. A. Crum, ''SWL cavitation damage *in vitro*: Pressurization unmasks a differential response of foil targets and isolated cells,'' Proc. 16th Intl. Congress on Acoustics, pp. 2497–2498 (1998).
[21] R. O. Cleveland, M. R. Bailey, L. A. Crum, M. A. Stonehill, J. C. Williams, and J. A. McAteer, ''Effect of overpressure on dissolution and cavitation of bubbles stabilized on a metal surface,'' Proc. 16th Intl. Congress on Acoustics, pp. 2499–2500 (1998).
[22] R. E. Apfel, ''Possibility of microcavitation from diagnostic ultrasound,'' IEEE Trans. Ultrason. Ferroelectr. Freq. Control **UFFC-33**, 139–142 (1986).
[23] C. K. Holland and R. E. Apfel, ''An improved theory for the prediction of microcavitation due to pulsed ultrasound,'' IEEE Trans. Ultrason. Ferroelectr. Freq. Control **UFFC-36**, 204–208 (1989).
[24] E. N. Harvey, ''Sonoluminscence and sonic chemiluminescence,'' J. Am. Chem. Soc. **61**, 2392–2398 (1939).
[25] R. D. Finch, ''The dependence of sonoluminescence on static pressure,'' Br. J. Appl. Phys. **16**, 1543–1553 (1965).
[26] P. K. Chendke and H. S. Fogler, ''Sonoluminescence and sonochemical reactions of aqueous carbon tetrachloride solutions,'' J. Phys. Chem. **87**, 1362–1369 (1983).
[27] J. Sponer, ''Dependence of ultrasonic cavitation threshold on raised ambient pressure,'' Stud. Biophys. **137**, 91–97 (1990).
[28] *Standard for the Real-Time Display of Thermal and Mechanical Acoustic Output Indices on Diagnostic Ultrasound Equipment* (American Institute of Ultrasound in Medicine, Laurel, MD, 1992, rev. 1996).
[29] K. Raum and W. D. O'Brien, Jr., ''Pulse-echo field distribution measurement technique of high-frequency ultrasound sources,'' IEEE Trans. Ultrason. Ferroelectr. Freq. Control **44**, 810–815 (1997).
[30] *Acoustic Output Measurement and Labeling Standard for Diagnostic Ultrasound Equipment* (American Institute of Ultrasound in Medicine, Laurel, MD, 1992).
[31] J. M. Sempsrott and W. D. O'Brien, Jr., ''Experimental verification of acoustic saturation,'' Proceedings of the 1999 IEEE Ultrasonics Symposium, pp. 1287–1290 (1999).
[32] G. A. Teotico, R. J. Miller, L. A. Frizzell, J. F. Zachary, and W. D. O'Brien, Jr., ''Attenuation coefficient estimates of mouse and rat chest wall,'' IEEE Trans. Ultrason. Ferroelectr. Freq. Control (in press).
[33] E. L. Madsen, F. Dong, G. R. Frank, B. S. Gara, K. A. Wear, T. Wilson, J. A. Zagzebski, H. L. Miller, K. K. Shung, S. H. Wang, E. J. Feleppa, T. Liu, W. D. O'Brien, Jr., K. A. Topp, N. T. Sanghvi, A. V. Zaitsen, T. J. Hall, J. B. Fowlkes, O. D. Kripfgans, and J. G. Miller, ''Interlaboratory comparison of ultrasonic backscatter, attenuation and speed measurements,'' J. Ultrasound Med. **18**, 615–631 (1999).
[34] D. W. Hosmer and S. Lemeshow, *Applied Logistic Regression* (Wiley, New York, 1989).
[35] J. Cohen and P. Cohen, *Applied Linear Regression/Analysis for the Behavioral Sciences* (Erlbaum, Hillsdale, NJ, 1983).
[36] M. L. Crosfill and J. G. Widdicombe, ''Physical characteristics of the chest and lungs and the work of breathing in different mammalian species,'' J. Physiol. (London) **158**, 1–14 (1961).
[37] S. M. Tenney and J. E. Remmers, ''Comparative quantitative morphology of the mammalian lung: Diffusing area,'' Nature (London) **197**, 54–56 (1963).
[38] E. R. Weibel, ''Dimensions of the tracheobronchial tree and alveoli,'' in *Biological Handbooks: Respiration and Circulation*, edited by P. L. Altman and D. S. Dittmer (Federation of American Societies for Experimental Biology, Bethedsa, MD, 1971), pp. 930–939.
[39] H. G. Flynn and C. C. Church, ''Transient pulsations of small gas bubbles in water,'' J. Acoust. Soc. Am. **84**, 985–998 (1988).
[40] M. R. Bailey, D. Dalecki, S. Z. Child, C. H. Raeman, D. P. Penney, D. T. Blackstock, and E. L. Carstensen, ''Bioeffects of positive and negative acoustic pressures *in vivo*,'' J. Acoust. Soc. Am. **100**, 3941–3946 (1996).
[41] E. L. Carstensen, D. Dalecki, S. M. Gracewski, and T. Christopher, ''Nonlinear propagation of the output indices,'' J. Ultrasound Med. **18**, 69–80 (1999).
[42] C. H. Raeman, S. Z. Child, D. Dalecki, C. Cox, and E. L. Carstensen, ''Exposure-time dependence of the threshold for ultrasonically induced murine lung hemorrhage,'' Ultrasound Med. Biol. **22**, 139–141 (1996).
[43] T. J. Bauld and H. P. Schwan, ''Attenuation and reflection of ultrasound in canine lung tissue,'' J. Acoust. Soc. Am. **56**, 1630–1637 (1974).
[44] F. Dunn, ''Attenuation and speed of ultrasound in lung,'' J. Acoust. Soc. Am. **56**, 1638–1639 (1974).